Ö. Sürücü / Hacettepe J. Biol. & Chem., 2020, 48 (2), 125-135

Research Article

Hacettepe Journal of Biology and Chemistry

journal homepage: www.hjbc.hacettepe.edu.tr

Electrodeposition of Cadmium Sulfide and Lead (II) Sulfide onto Polycrystalline Gold Electrode

Polikristalin Altın Elektrot Üzerine Kadmiyum Sülfür ve Kurşun (II) Sülfürün Elektrodepozisyonu

Özge Sürücü[1,2]

[1]Department of Chemistry, Faculty of Science, Hacettepe University, Ankara, Turkey.

[2]Department of Chemistry, Faculty of Science, Ege University, Izmir, Turkey.

ABSTRACT

A new, simple and cost-effective electrochemical route was demontrated in this work. CdS and PbS thin films were grown on polycrystalline gold electrode using co-deposition and ECALE techniques based on accumulation layer by layer. The deposition potentials of cadmium, lead and sulfur were determined separately by cyclic voltammetry. Thin films were created from an electrolyte containing 0.01 molL^{-1} $CdSO_4$, 0.01 molL^{-1} Na_2S and 0.01 molL^{-1} $Pb(CH_3COO)_2$ in 0.01 molL^{-1} EDTA (pH = 3.00). The influence of bath temperature at the deposition potential was studied to determine the crystallinity of deposits. From the chronoamperometry results including the transients which were obtained within the under potential region, the overall shape of the experimental depositions was proposed and the growth process was considered.

Key Words

Underpotential deposition, co-deposition, ECALE.

ÖZ

Bu çalışmada yeni, basit ve uygun maliyetli bir elektrokimyasal rutin gösterildi. CdS ve PbS ince filmler polikristalin altın elektrot üzerinde tabaka tabaka biriktirme temeliyle ko-depozisyon ve ECALE teknikleri kullanılarak büyütüldü. Kadmiyum, kurşun ve kükürdün biriktirme potansiyelleri ayrı ayrı dönüşümlü voltametri ile belirlendi. İnce filmler 0.01 molL^{-1} EDTA'da (pH = 3.00) 0.01 molL^{-1} $CdSO_4$, 0.01 molL^{-1} Na_2S ve 0.01 molL^{-1} $Pb(CH_3COO)_2$ içeren elektrolitten oluşturuldular. Biriktirme potansiyelindeki sıcaklık etkisi birikintilerin kristalliğinin belirlenmesi için çalışıldı. Potansiyel altı alanı içerisinde elde edilen geçişleri kapsayan kronoamperometri sonuçlarından, deneysel birikimlerin genel şekilleri önerildi ve büyüme süreci değerlendirildi.

Anahtar Kelimeler

Potansiyel altı biriktirme, ko-depozisyon, ECALE.

Article History: Received: Feb 19, 2019; Revised: Dec 16, 2019; Accepted: Dec 20, 2019; Available Online: Apr 1 , 2020.

DOI: https://doi.org/10.15671/hjbc.529104

Correspondence to: Ö. Sürücü, Department of Chemistry, Faculty of Science, Hacettepe University, Ankara, Turkey.

E-Mail: ozge87@hacettepe.edu.tr

INTRODUCTION

Cadmium (Cd) and lead (Pb) are electroactive heavy metals, so they can be detected electrochemically. The monitoring of Cd and Pb using sensitive, inexpensive and portable electrochemical methods is an attractive way to determine hazardous heavy metals [1]. At the same time, II-VI semiconductors like cadmium sulfide (CdS) have a wide application in the non-linear optical materials, solar cells, light-emitting diodes, electronic and optoelectronic devices [2] and IV-VI semiconductors like lead (II) sulfide (PbS) are also focused on field-effect thin film transistors, single-electron transistors and flat-panel displays [3]. In such an important field, deposition of these materials is coming into prominence and electrochemistry is a good alternative to conventional deposition methods with a number of advantages such as film thickness control, operation at ambient temperature and pressure [4, 5].

Under potential deposition (UPD) is an electrodeposition technique based on the reduction of a metal cation to a solid metal at a more positive potential than the equilibrium (Nernst) potential for the reduction of this metal [6]. UPD is generally occurs as a result of a strong interaction between the electrodepositing metal (M) and the substrate (S) which is used to construct the electrode. The M-S interaction must be energetically active to the M-M interaction in the crystal lattice of the pure M. Such a process is developed by the observation of UPD which can occur up to a monolayer or two monolayers of M. The reference point for the UPD is characterized by the electrodeposition of M on a S of the same M taking place at an equilibrium potential [7].

As one of the UPD method, electrolytic co-deposition is an electroplating method which consists of the mixing of non-metallic particles into metallic coatings obtained from electrolytes containing the particles in a suspended state [8]. The second phase particles like ethylenediaminetetraacetic acid (EDTA) which dispersed within the metal base such as Cd and Pb form a metal matrix composite (CdEDTA2- and PbEDTA2-) and these composites may show different properties from those of the pure metallic deposits (Cd^{2+} and Pb^{2+}). This method is widely applied to create CdS [9] and PbS [10] thin films in single-crystalline forms, but a little effort is made to overcome the problem of polycrystalline deposits.

Electrochemical atomic layer epitaxy (ECALE) is an atomic layer deposition technique based on UPD where an atomic layer of the element is deposited on the surface by an electrochemical surface limited reaction using an electrochemical cell, at an electrode potential lower than it is needed to deposit the element on itself [11]. In ECALE of CdS and PbS: an atomic layer of cadmium or lead is deposited, followed by an atomic layer of sulfur deposition on the cadmium or lead, and then one of cadmium or lead is again deposited on the sulfur as proposed by Stickney [12].

In this work, the electrodepositions of cadmium and lead together with sulfur onto polycrystalline gold electrode were compared using various techniques including co-deposition and ECALE for the first time. Bulk electrolysis and cyclic voltammetry techniques were applied to determine key parameters such as the deposition potential, deposition time and the effect of temperature. At the same time, chronoamperometry method was used to define the dimensionality of the resulting deposits. The present work mainly aims using of polycrystalline surfaces instead of single crystal surfaces which possess a time-consuming preparation procedure to detect not only hazardous heavy metals, but also to create binary systems and thin films by proposed practical new approach.

MATERIALS and METHODS

Chemicals

Before starting the analysis, gold electrode was mechanically polished with 0.05 and 1.00 μm superfine alumina (Al_2O_3) powders and then cleaned electrochemically with successive cycling in 1.00 $molL^{-1}$ sulphuric acid (H_2SO_4) solution from Sigma-Aldrich between -0.20 V and +1.50 V versus Ag/AgCl until a steady state current was obtained. The prepared 0.01 $molL^{-1}$ EDTA at pH = 3.00 was used as a supporting electrolyte. Cadmium sulfate ($CdSO_4$), sodium sulfide (Na_2S) and lead (II) acetate ($Pb(CH_3COO)_2$) solutions from Sigma-Aldrich were prepared in the concentration amount of 0.01 $molL^{-1}$. All the other reagents were in analytical grade. At the beginning of analysis, pure N_2 gas was passed from all of the prepared solutions for sufficient period of time to extract oxygen.

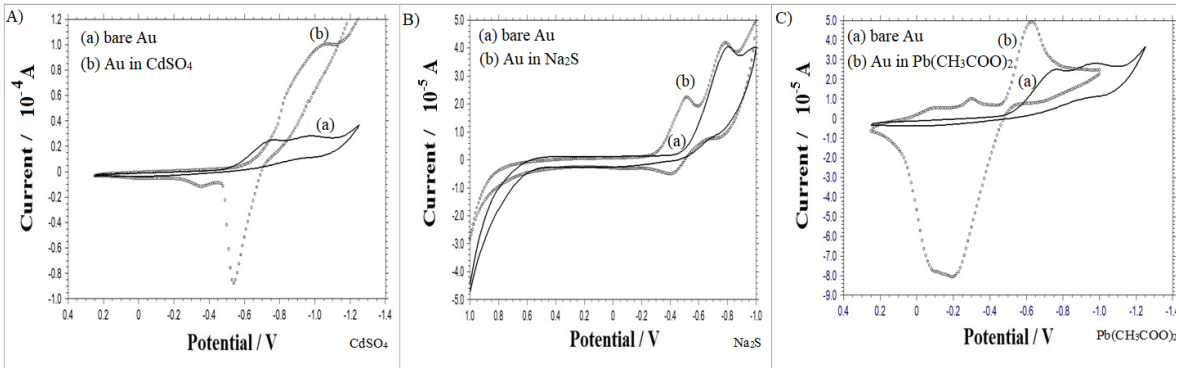

Figure 1. Cyclic voltammograms of bare Au in 0.01 molL^{-1} EDTA (a), and Au in 0.01 molL^{-1} EDTA containing A) 0.01 molL^{-1} $CdSO_4$ between +0.25 V and -1.25 V versus Ag/AgCl, B) 0.01 molL^{-1} Na_2S between +1.00 V and -1.00 V versus Ag/AgCl, C) 0.01 molL^{-1} $Pb(CH_3COO)_2$ between +0.25 V and -1.25 V versus Ag/AgCl (b), at a scan rate of 100 mV s^{-1}.

Instruments

Bulk electrolysis and cyclic voltammetry techniques were performed on CH Instruments CHI660C model potentiostat in the three electrode setup for electrochemical cells comprising platinum (Pt) wire as the counter electrode, silver/silver chloride (Ag/AgCl) as the reference electrode and gold (Au) electrode with 0.03 cm² area as working electrode. Bulk electrolysis was done at -0.35 V versus Ag/AgCl for Cd, -0.52 V versus Ag/AgCl for S and -0.10 V for Pb versus Ag/AgCl for 10 minutes. Cyclic voltammetry was applied between +0.25 V and -1.60 V versus Ag/AgCl for 10 cycles, and the direction of potential scan was from negative to positive. Chronoamperometry technique was performed between +0.10 V and -0.35 V versus Ag/AgCl for Cd, +0.60 V and -0.43 V versus Ag/AgCl for Pb.

Mechanism of co-deposition and ECALE of cadmium sulfide and lead (II) sulfide

In the mechanism of co-deposition, the second phase particles (EDTA) suspended in the electrolyte adsorb the positively charged metal ions (Cd^{2+} and Pb^{2+}). The metal ions enclose the EDTA particles and the resulting complexes ($CdEDTA^{2-}$ and $PbEDTA^{2-}$) arrive at the cathode taking action by the electrostatic attraction and the electrolyte convection. The particles stayed at the cathode surface discharge and the three related interfacial energies including particle-electrolyte, particle-cathode and cathode-electrolyte help to retain the particles on the surface by the bonding force. The metal ions are deposited on the cathode surface around the particles mixing into the metallic deposits. In the case of sulfur, anodic deposition is obtained on the anode surface.

Each pair of elements has its own UPD chemistry and it must be investigated to discover its proper ECALE cycle. Such a cycle is the sequence of steps used to deposit one stoichiometric layer of the targeted element which can be an atomic layer for a pure element, or a bi-layer of a 1:1 compound. CdS or PbS cycle is composed of several steps: initially a reductive UPD of cadmium or lead from a cadmium or lead cation solution, then oxidative UPD of sulfur from a sulfide anion solution, and finally a second reductive UPD of cadmium or lead from a cadmium or lead cation solution. Separate solutions are used for each material and different potentials for each cycle step. The use of separate solutions and potentials has a lot of advantages such as extensive control over deposit growth, composition and morphology. At the same time, it is avoided from the oxidation of metal surface before sulfurization by means of each species own potential. The cycle is repeated to form a thin film because the deposit thickness is a linear function of the number of cycles. Such a linear relation is a good indication of a layer by layer mechanism, and an atomic layer deposition process.

RESULTS and DISCUSSION

UPD of cadmium, sulfur and lead

The formation of the first monolayer is inferred from the declared current peaks at the potential $E > E_{rev}$ while the bulk deposition occurs at $E < E_{rev}$ where E_{rev} specifies the Nernstian equilibrium potential [13]. As it is known, E_{rev} is –0.46 V versus Ag/AgCl for Cd/Cd^{2+} and –0.19 V versus Ag/AgCl for Pb/Pb^{2+}. In (Figure 1 A), cyclic voltammogram

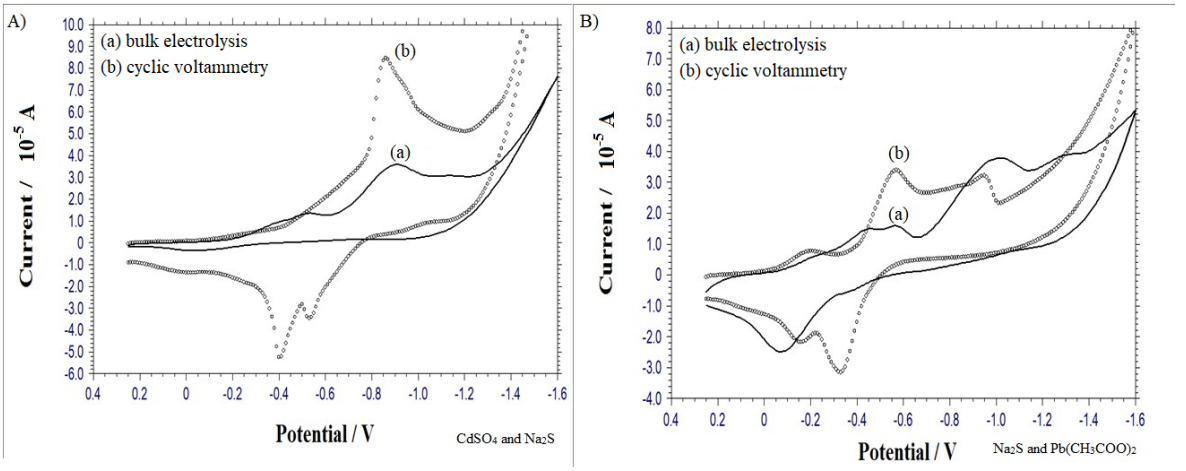

Figure 2. Cyclic voltammograms of bulk electrolyzed Au for 10 minutes (a), and coated Au for 10 cycles (b) in A) 0.01 molL^{-1} EDTA containing 0.01 molL^{-1} $CdSO_4$ and 0.01 molL^{-1} Na_2S and B) 0.01 molL^{-1} EDTA containing 0.01 molL^{-1} Na_2S and 0.01 molL^{-1} $Pb(CH_3COO)_2$ between +0.25 and -1.60 V versus Ag/AgCl at a scan rate of 100 mV s^{-1}.

of Au electrode in 0.01 molL^{-1} EDTA containing 0.01 molL^{-1} $CdSO_4$ was compared with bare Au electrode behavior in 0.01 molL^{-1} EDTA, and bulk potential of Cd was obtained at –0.55 V (less than –0.46 V) versus Ag/AgCl, UPD potential at –0.35 V (more than –0.46 V) versus Ag/AgCl [14]. In (Figure 1 C), cyclic voltammogram of Au electrode in 0.01 molL^{-1} EDTA containing 0.01 molL^{-1} $Pb(CH_3COO)_2$ was compared with bare Au electrode behavior in 0.01 molL^{-1} EDTA. A broad peak was observed between –0.20 V and 0.00 V versus Ag/AgCl, but two side by side peaks were actually gained. Bulk potential of Pb was obtained at –0.23 V (less than –0.19 V) versus Ag/AgCl, UPD potential at –0.10 V (more than –0.19 V) versus Ag/AgCl [15]. In the case of S, cyclic voltammogram of Au electrode in 0.01 molL^{-1} EDTA containing 0.01 molL^{-1} Na_2S was compared with bare Au electrode behavior in 0.01 molL^{-1} EDTA, but anodic potentials were estimated instead of cathodic potentials (Figure 1 B). The bulk potential of S was obtained at –1.00 V versus Ag/AgCl, UPD potential at –0.52 V versus Ag/AgCl and all results were essentially identical to that reported in literature [16].

Bulk electrolysis versus cyclic voltammetry

After the determination of UPD potentials of Cd, S and Pb, the deposition of species were made using both bulk electrolysis and cyclic voltammetry techniques. Bulk electrolysis was applied at –0.35 V versus Ag/AgCl for Cd, –0.52 V versus Ag/AgCl for S, –0.10 V versus Ag/AgCl for Pb for 10 minutes while cyclic voltammetry was applied between +0.25 and –1.60 V versus Ag/AgCl for 10 cycles. The methodological difference in the voltammetric behavior of Au electrode in 0.01 molL^{-1} EDTA containing 0.01 molL^{-1} $CdSO_4$ and 0.01 molL^{-1} Na_2S (Figure 2 A) and in 0.01 molL^{-1} EDTA containing 0.01 molL^{-1} Na_2S and 0.01 molL^{-1} $Pb(CH_3COO)_2$ (Figure 2 B) was determined, and the UPD peaks of Cd, S and Pb were lost in the event of bulk electrolysis. Therefore, the layer formation was performed by increasing number of cycle. The phase purities of CdS and PbS deposited on polycrystalline Au electrode were uniform, so flower-like structures were proposed at long-deposition times [17].

Co-deposition versus ECALE

Cyclic voltammetric responses of Au electrode using co-deposition method based on deposition from the same solution of the precursors of the target compound at a constant UPD potential, and using ECALE method based on deposition of each element from their separate solutions at the UPD potential of each element were represented in (Figure 3). In co-deposition method (a), S UPD (–0.52 V versus Ag/AgCl) disappeared, but in ECALE behavior of S over Cd modified Au electrode (c), both Cd (–0.35 V versus Ag/AgCl) and S UPD peaks were observed by a sharper result than Cd over S modified Au electrode (b) presenting the layer formation of S over Cd modified Au electrode (Figure 3A). In the mechanism of CdS electrodeposition, Cd reduction ($Cd^{2+} + 2e^-$ = Cd(UPD)) and S oxidation (S^{2-} = S(UPD) + $2e^-$) occured as 1:1. An atomic layer of S was deposited on one of Cd, and one of Cd was deposited on one of S.

In the case of Pb and S co-deposition method (a), both Pb and S UPD peaks were monitored at the actual UPD potentials of Pb (–0.10 V versus Ag/AgCl) and S (–0.52 V

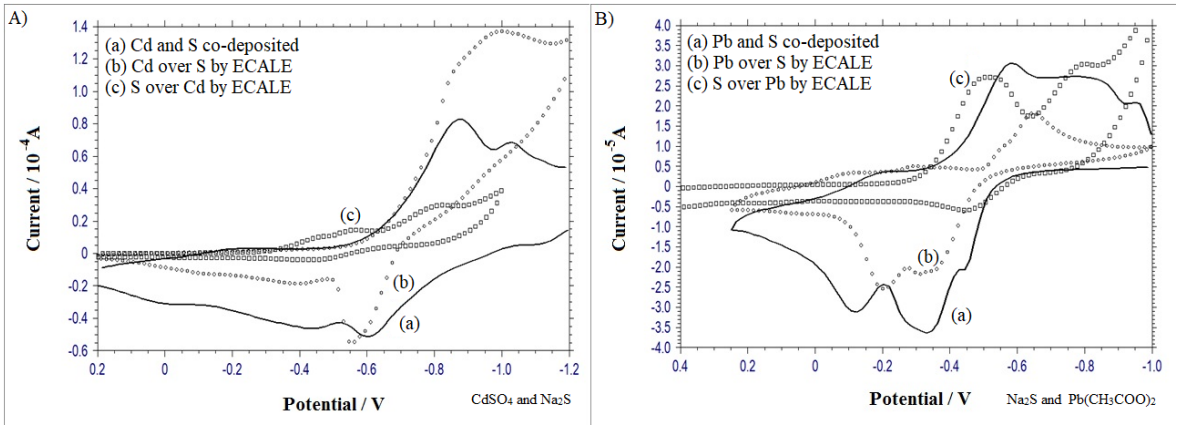

Figure 3. Cyclic voltammograms of coated Au for 10 cycles in A) 0.01 molL^{-1} EDTA containing 0.01 molL^{-1} $CdSO_4$ and 0.01 molL^{-1} Na_2S using (a) Cd and S by co-deposition, (b) Cd over S by ECALE, (c) S over Cd by ECALE techniques, and B) 0.01 molL^{-1} EDTA containing 0.01 molL^{-1} Na_2S and 0.01 molL^{-1} $Pb(CH_3COO)_2$ using (a) Pb and S by co-deposition, (b) Pb over S by ECALE, (c) S over Pb by ECALE techniques between +0.25 and -1.60 V versus Ag/AgCl at a scan rate of 100 mV s^{-1}.

versus Ag/AgCl), but in ECALE result of Pb over S modified Au electrode (b), UPD potential of Pb shifted more negative potential (–0.20 V versus Ag/AgCl) weakening the interactions of Pb with the substrate [18], and in S over Pb modified Au electrode response by ECALE (c), Pb UPD was lost (Figure 3B). Therefore, PbS layer was created using co-deposition technique from the same solutions of Pb and S. In the mechanism of PbS electrodeposition, Pb reduction ($Pb^{2+} + 2e^- = Pb(UPD)$) and S oxidation ($S^{2-} = S(UPD) + 2e^-$) occured as 1:1. An atomic layer of S was deposited on one of Pb, and one of Pb was deposited on one of S.

The effect of bath temperature on UPD

The influence of bath temperature on UPD was studied and the bath temperature was varied from 25°C to 40°C to examine the change of composition and microstructure of the deposits. In (Figure 4), the current intensities of bare Au electrode in 0.01 molL^{-1} EDTA containing 0.01 molL^{-1} $CdSO_4$ A), S over Cd modified Au electrode B), and Cd and S co-deposited Au electrode C) in 0.01 molL^{-1} EDTA containing 0.01 molL^{-1} $CdSO_4$ and 0.01 molL^{-1} Na_2S were compared. When the bath temperature was increased from 25°C to 40°C (d→a), the potentials shifted to more positive direction, the intensity of the peaks increased gradually for both bare Cd A) and S over Cd B) behaviors, particularly at 40°C the current rised from 6.6×10^{-5} A to 7.4×10^{-5} A obviously. In the case of Cd and S co-deposition C), the peak current at 30°C reached its maximum value randomly and a general roll-off rate was observed. Therefore, the layer formation of CdS was carried out using ECALE technique as in UPD results of S over Cd modified Au electrode, and the increase of the bath temperature improved the crystallinity of the CdS deposit [19].

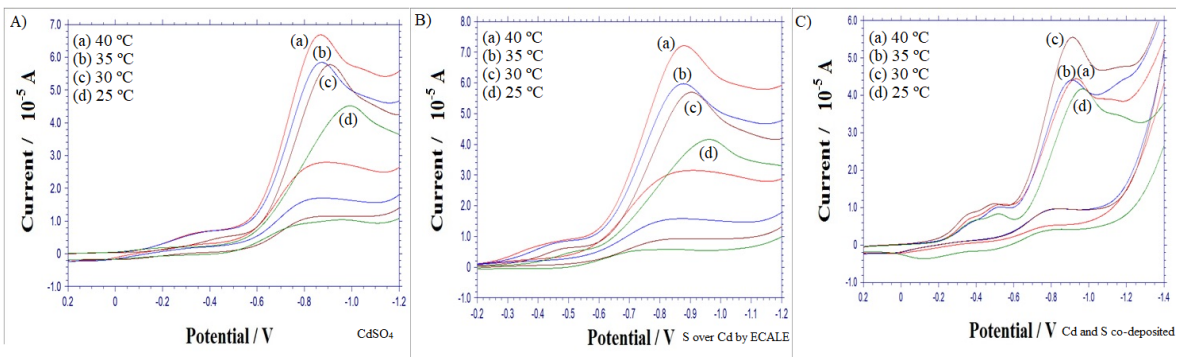

Figure 4. Cyclic voltammograms of coated Au for 10 cycles A) in 0.01 molL^{-1} EDTA containing 0.01 molL^{-1} $CdSO_4$, B) using S over Cd by ECALE, C) using Cd and S by co-deposition techniques in 0.01 molL^{-1} EDTA containing 0.01 molL^{-1} $CdSO_4$ and 0.01 molL^{-1} Na_2S between +0.25 and -1.60 V versus Ag/AgCl at a scan rate of 100 mV s^{-1}, and at a bath temperature of (a) 4°C, (b) 35°C, (c) 30°C, (d) 25°C.

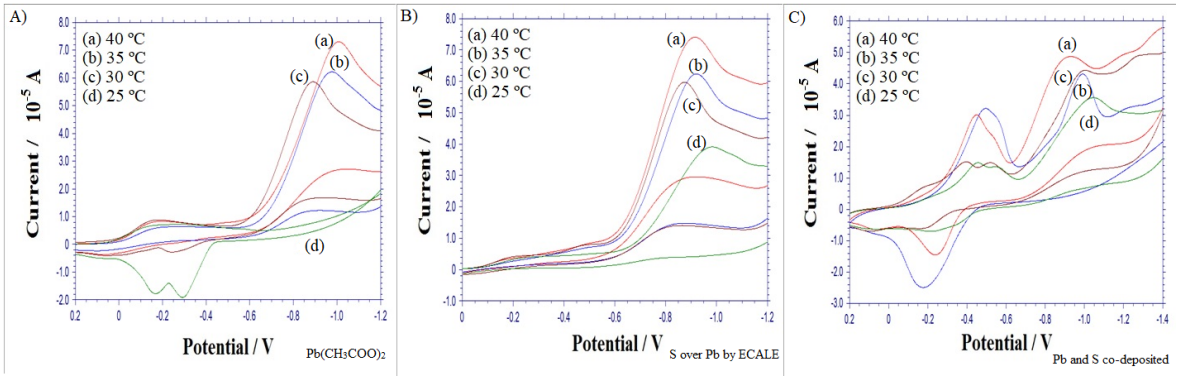

Figure 5. Cyclic voltammograms of coated Au for 10 cycles A) in 0.01 molL^{-1} EDTA containing 0.01 molL^{-1} $Pb(CH_3COO)_2$, B) using S over Pb by ECALE, C) using Pb and S by co-deposition techniques in 0.01 molL^{-1} EDTA containing 0.01 molL^{-1} $Pb(CH_3COO)_2$ and 0.01 molL^{-1} Na_2S between +0.25 and -1.60 V versus Ag/AgCl at a scan rate of 100 mV s^{-1}, and at a bath temperature of (a) 40°C, (b) 35°C, (c) 30°C, (d) 25°C.

(Figure 5) demonstrated the current intensity changes of bare Au electrode in 0.01 molL^{-1} EDTA containing 0.01 molL^{-1} $Pb(CH_3COO)_2$ A), S over Pb modified Au electrode B), and Pb and S co-deposited Au electrode C) in 0.01 molL^{-1} EDTA containing 0.01 molL^{-1} $Pb(CH_3COO)_2$ and 0.01 molL^{-1} Na_2S. As the bath temperature increased from 25°C to 40°C (d→a), the intensity of the peaks increased gradually for both bare Pb A) and S over Pb B) behaviors. When Pb UPD peak at –0.10 V versus Ag/AgCl was taken into account, no peak was observed for S over Pb modified Au electrode B). At the lower bath temperatures (c, d), the content of elemental Pb was slightly greater than that of S A) reaching its current maximum (–1.80 × 10^{-5} A) and at the higher bath temperatures (a, b) the content of elemental Pb (–2.60 × 10^{-5} A) was slightly less than that of S (+3.40 × 10^{-5} A) C). Therefore, the layer formation of PbS was carried out using co-deposition technique as in UPD results of Pb and S co-deposited Au electrode, and the bath temperature had an influence on the composition of the deposited films.

Kinetics of the electrodepositions

Electrodeposition takes place by a process of nucleation which appears at active sites on the substrate due to nucleation rate law, and growth which occurs by growing via the incorporation of further ions from the solution. Nucleation and growth can be divided into sub-categories such as interfacial controlled and diffusion controlled. In the former, the nucleus growth rate is limited by the speediness at which ions can be incorporated into the new phase. In the later, nucleus growth is limited by the rate at which material is transported through the solution to the electrode surface [20].

The number of various models has been proposed to decide the dominance of adsorption-desorption or nucleation and growth on the chronoamperometric response of systems. Among these models, the evaluation of the current density as the sum of two independent terms, a Langmuir type adsorption-desorption term and a nucleation growth term ($j_{total} = j_{ads} + j_{nucl/growth}$) is the simplest one. Such an approach can be applied on the basis where adsorption is typically a rapid process, while nucleation and growth develop more slowly due to kinetic limitations. In the Butler-Volmer model, adsorption-desorption is followed by surface diffusion control of monolayer nucleation and growth [21]. In cases where the two processes are not decoupled, a more complex model such as that of Bosco and Rangarajan is required [22].

In (Figure 6), chronoamperometric results of bare Au A), and coated Au for 10 cycles B) in 0.01 molL^{-1} EDTA containing 0.01 molL^{-1} $CdSO_4$, coated Au for 10 cycles using Cd and S by co-deposition C), and coated Au for 10 cycles using Cd over S by ECALE D) techniques in 0.01 molL^{-1} EDTA containing 0.01 molL^{-1} $CdSO_4$ and 0.01 molL^{-1} Na_2S were estimated. In all conditions, the current density (j) decreased as a function of elapsing time (t < 0.03 s), right from the start of the transient resulted in no nucleation model giving a clear description of the transient shape. For t > 0.03 s, the shape of transient supported the formation and growth of 2D nuclei, limited by ad-atom incorporation. As it could be seen in (Figure 6) from B) to D), a current enhancement appeared in Cd monolayer formation and it proceeded by a two-step mechanism involving Langmuir-type adsorption accompanied by nucleation and two dimensional growth. Therefore, Cd deposition was described by the

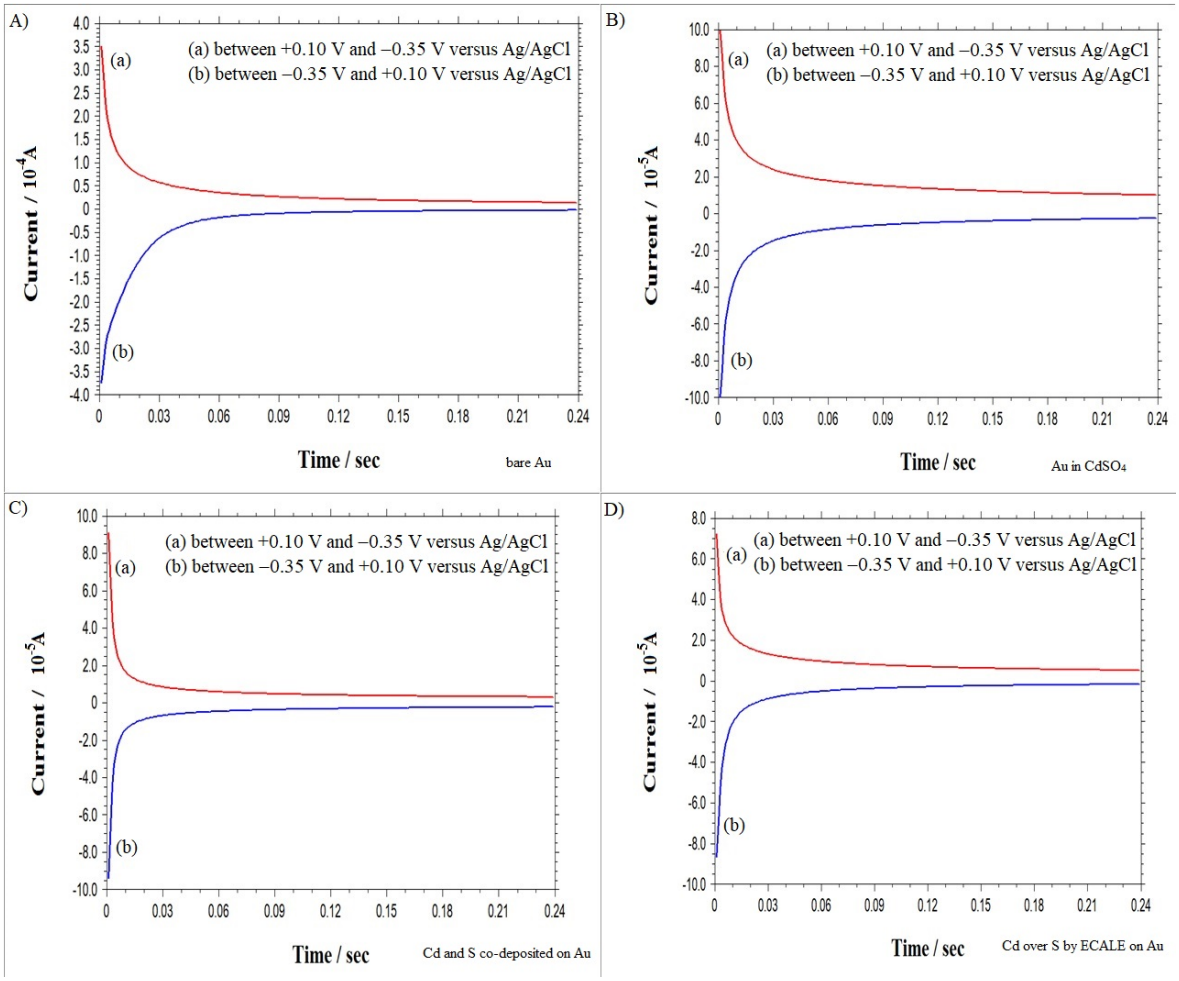

Figure 6. Chronoamperometric behaviors of A) bare Au, B) coated Au for 10 cycles in 0.01 molL^{-1} EDTA containing 0.01 molL^{-1} $CdSO_4$, C) coated Au for 10 cycles using Cd and S by co-deposition, D) coated Au for 10 cycles using Cd over S by ECALE techniques in 0.01 molL^{-1} EDTA containing 0.01 molL^{-1} $CdSO_4$ and 0.01 molL^{-1} Na_2S between (a) +0.10 V and -0.35 V versus Ag/AgCl and (b) -0.35 V and +0.10 V versus Ag/AgCl.

model ($j_{total} = j_{AD} + j_{2D}$) used by Hölzle et al. [23] in which the electrodeposition process (j_{total}) was the linear sum of a Langmuir-type adsorption term (j_{AD}) and a 2D nucleation process (j_{2D}).

In order to analyze the experimental data by usual procedures, the plots of I versus $t^{1/2}$ for bare Au A) and coated Au for 10 cycles B) in 0.01 molL^{-1} EDTA containing 0.01 molL^{-1} $CdSO_4$, coated Au for 10 cycles using Cd and S by co-deposition C), and coated Au for 10 cycles using Cd over S by ECALE D) techniques in 0.01 molL^{-1} EDTA containing 0.01 molL^{-1} $CdSO_4$ and 0.01 molL^{-1} Na_2S recorded between (a) +0.10 V and –0.35 V versus Ag/AgCl and (b) –0.35 V and +0.10 V versus Ag/AgCl were given in (Figure 7).

The resulting straight line in all curves (Table 1) showed a diffusion-controlled process according to the Cottrell equation [24] and the higher the slope of graph was obtained in (Figure 7 A) because of the metal ion behavior of Au. For the electrodeposition of Cd from B) to D), the slopes namely diffusion coefficients ($D \sim 1/\eta$) reduced normally because of the absolute viscosity (η) which was greater for thin films in comparison with free metals.

For the higher potentials, nucleation and growth properties come forward in the chronoamperometry; the reduction current increases until it reaches a maximum with a later decline with time and diffusion becomes the rate-limiting process. Different nucleation and

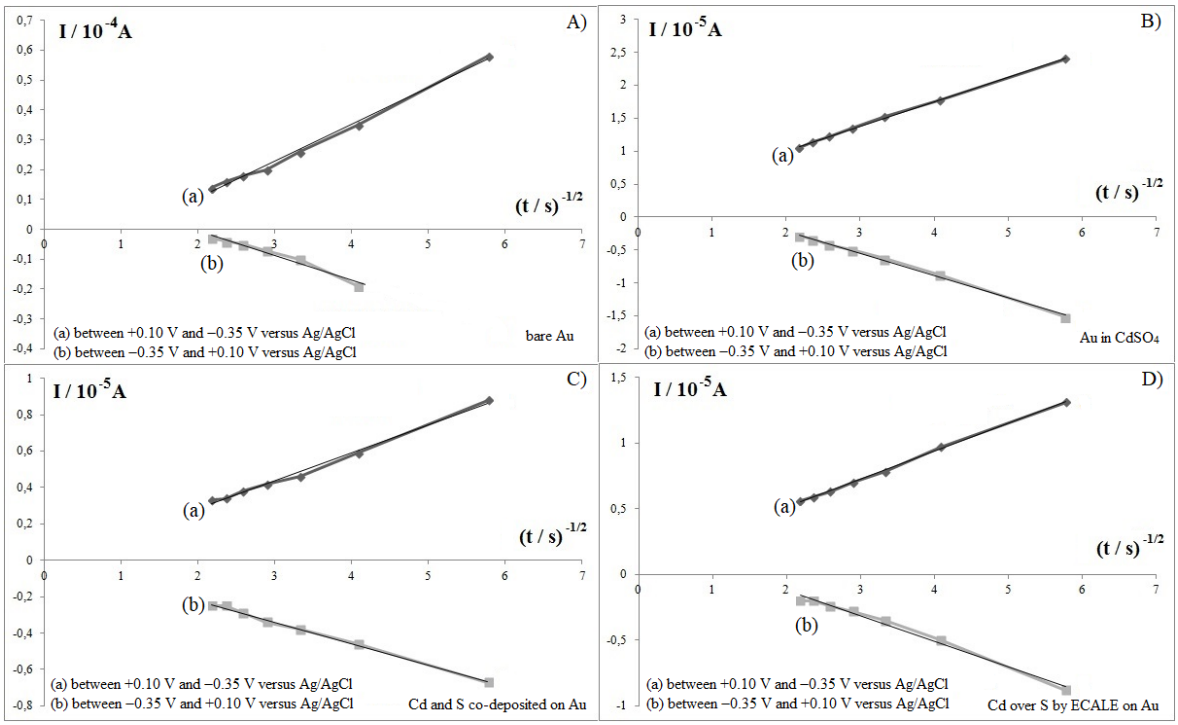

Figure 7. The plots of I versus $t^{-1/2}$ indicating the current transients of bare Au A), coated Au for 10 cycles B), coated Au for 10 cycles using Cd and S by co-deposition C), and coated Au for 10 cycles using Cd over S by ECALE D) recorded between two potential ranges (+0.10 V - (-0.35 V) versus Ag/AgCl and -0.35 V – (+0.10 V) versus Ag/AgCl), see in (Figure 6). Two lines surrounding markers showed the linearity (R^2 in Table 1) and straight line passing through the points.

growth mechanisms were considered in the analysis of the potential step data, and the experimental data was found to be best described using the 3D instantaneous, diffusion-controlled nucleation and growth mechanism [25].

(Figure 8) represented chronoamperometric responses of bare Au A) and coated Au for 10 cycles B) in 0.01 molL^{-1} EDTA containing 0.01 molL^{-1} $Pb(CH_3COO)_2$, coated Au for 10 cycles using Pb and S by co-deposition C), and coated Au for 10 cycles using Pb over S by ECALE D) techniques in 0.01 molL^{-1} EDTA containing 0.01 molL^{-1} $Pb(CH_3COO)_2$ and 0.01 molL^{-1} Na_2S. A current decline from A) to C) was observed by Pb monolayer formation, but when Pb monolayer was formed over S modified Au electrode D), the current increased again. It proceeded by a two-step mechanism involving 3D instantaneous, diffusion-controlled nucleation and growth mechanism.

In (Figure 9), the plots of I versus $t^{1/2}$ and $t^{-1/2}$ for bare Au A) and coated Au for 10 cycles B) in 0.01 molL^{-1} EDTA containing 0.01 molL^{-1} $Pb(CH_3COO)_2$, coated Au for 10 cycles using Pb and S by co-deposition C), and coated Au for 10 cycles using Pb over S by ECALE D) techniques in 0.01 molL^{-1} EDTA containing 0.01 molL^{-1} $Pb(CH_3COO)_2$ and 0.01 molL^{-1} Na_2S recorded between +0.60 V and (a) –0.43 V versus Ag/AgCl, (b) –0.44 V versus Ag/AgCl, (c) –0.45 V versus Ag/AgCl, (d) –0.46 V versus Ag/AgCl were indicated.

Table 1. Equations and coefficients of determination for the plots of I versus $t^{-1/2}$

Potential Range (V)	Bare Au	Au in $CdSO_4$	Cd and S co-deposited on Au	Cd over S by ECALE on Au
+0.10 – (-0.35)	y=0.1228x–0.1396 R^2=0.9943	y=0.3714x+0.2626 R^2=0.9991	y=0.1541x–0.0247 R^2=0.9928	y=0.2121x+0.0888 R^2=0.9986
-0.35 – (+0.10)	y=–0.0826x+0.1599 R^2=0.9656	y=–0.3408x+0.4747 R^2=0.9965	y=–0.1183+0.0148 R^2=0.9963	y=–0.1930x+0.2610 R^2=0.9878

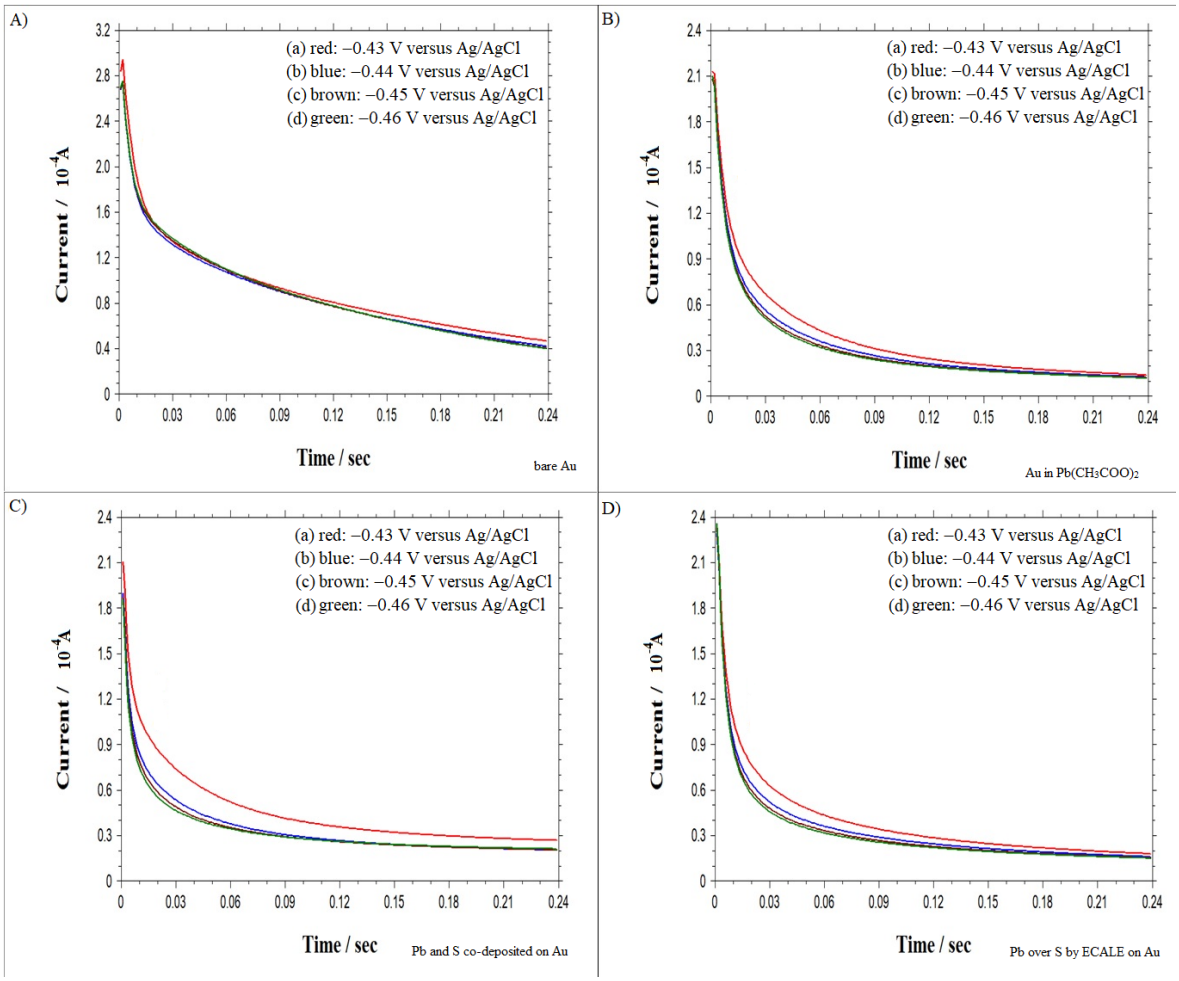

Figure 8. Chronoamperometric behaviors of A) bare Au, B) coated Au for 10 cycles in 0.01 molL^{-1} EDTA containing 0.01 molL^{-1} $Pb(CH_3COO)_2$, C) coated Au for 10 cycles using Pb and S by co-deposition, D) coated Au for 10 cycles using Pb over S by ECALE techniques in 0.01 molL^{-1} EDTA containing 0.01 molL^{-1} $Pb(CH_3COO)_2$ and 0.01 molL^{-1} Na_2S between +0.60 V and (a) -0.43 V versus Ag/AgCl, (b) -0.44 V versus Ag/AgCl, (c) -0.45 V versus Ag/AgCl, (d) -0.46 V versus Ag/AgCl

For only (Figure 9 A), the graph of I versus $t^{1/2}$ was drawn because of the bent curve of I versus $t^{-1/2}$, and the resulting linearity was obtained by the bare Au (Table 2). For the electrodeposition of Pb from B) to D), the diffusion coefficients ($D \sim 1/\eta$) based on the slopes declined normally because of the absolute viscosity (η) which was greater for deposits in comparison with free metals B).

Conclusion

A simple and new route for the electrodeposition of CdS and PbS based on co-deposition and ECALE techniques was improved as a one-step and cost-effective process. Two different methods to produce semiconducting materials were examined in detail onto polycrystalline electrodes for the first time. Various electrochemical deposition processes such as bulk electrolysis and cyclic voltammetry were used to determine the best layer formation. The effect of bath temperature on UPD was studied to estimate the quality and crystallinity of deposits, and the temperature results were in a good correlation with UPD responses of CdS and PbS. To decide the kinetic behaviors of deposits, another electrochemical technique namely which was chronoamperometry was performed, and two-step mechanism involving adsorption accompanied by nucleation and growth was obtained. In summary, UPD was applied on both pure metals and deposits by means of this work,

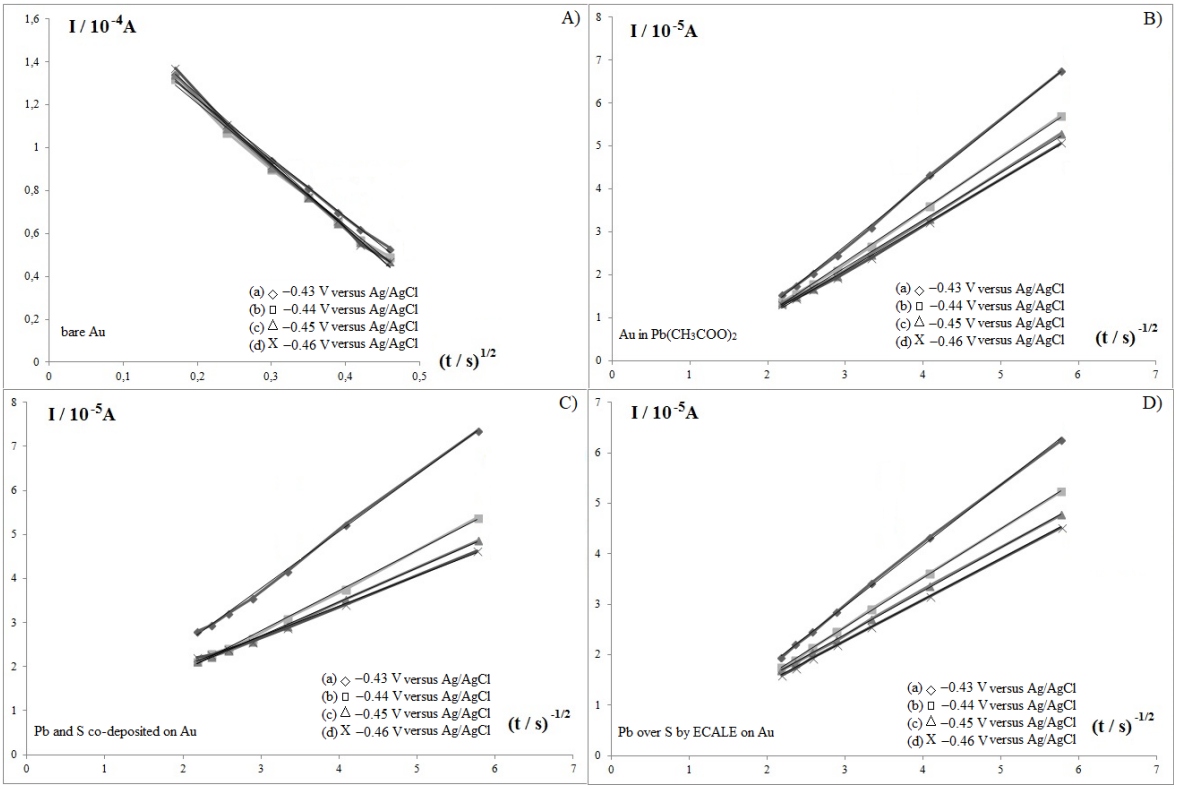

Figure 9. The plots of I versus t½ and t-½ indicating the current transients of bare Au A), coated Au for 10 cycles B), coated Au for 10 cycles using Pb and S by co-deposition C), and coated Au for 10 cycles using Pb over S by ECALE D) recorded between four potential ranges (+0.60 V - (-0.43 V), (-0.44 V), (-0.45 V), (-0.46 V) versus Ag/AgCl), see in (Figure 8). Two lines surrounding markers showed the linearity (R^2 in Table 2) and straight line passing through the points.

Table 2. Equations and coefficients of determination for the plots of I versus $t^{1/2}$ and I versus $t^{-1/2}$.

Potential Range (V)	Bare Au	Au in $Pb(CH_3COO)_2$	Pb and S co-deposited on Au	Pb over S by ECALE on Au
+0.60 - (-0.43)	y=-2.7545x+1.7783 R^2=0.9955	y=1.4679x-1.7302 R^2=0.9992	y=1.2905x-0.0938 R^2=0.9989	y=1.1969x-0.6208 R^2=0.9993
+0.60 - (-0.44)	y=-2.8487x+1.7739 R^2=0.9651	y=1.2163x-1.345 R^2=0.9993	y=0.9104x+0.0869 R^2=0.9983	y=0.9748x-0.3780 R^2=0.9997
+0.60 - (-0.45)	y=-3.1131x+1.8719 R^2=0.9959	y=1.1062x-1.1462 R^2=0.9982	y=0.7709x+0.3862 R^2=0.9987	y=0.8615x-0.1841 R^2=0.9998
+0.60 - (-0.46)	y=-2.9971x+1.8247 R^2=0.9969	y=1.0583x-1.0759 R^2=0.9987	Y=0.6849x+0.6410 R^2=0.9973	y=0.8143x-0.1690 R^2=0.9999

so the proposed method may serve as a model for semi-conducting industry and environmental science.

References

1. T. Noyhouzer, D. Mandler, Determination of low levels of cadmium ions by the under potential deposition on a self-assembled monolayer on gold electrode, Anal. Chim. Acta, 684 (2011) 1-7.
2. T. Peng, H. Yang, K. Dai, X. Pu, K. Hirao, Fabrication and characterization of CdS nanotube arrays in porous anodic aluminum oxide templates, Chem. Phys. Lett., 379 (2003) 432-436.
3. M. Alanyalıoğlu, F. Bayrakçeken, Ü. Demir, Preparation of PbS thin films: A new electrochemical route for underpotential deposition, Electrochim. Acta, 54 (2009) 6554-6559.
4. M.M. Momeni, A.A. Mozafari, The effect of number of SILAR cycles on morphological, optical and photo catalytic properties of cadmium sulfide–titania films, J. Mater. Sci.-Mater. El., 27 (2016) 10658-10666.
5. M.M. Momeni, M. Mahvari, Y. Ghaveb, Photoelectrochemical properties of iron-cobalt WTiO2 nanotube photoanodes for water splitting and photocathodic protection of stainless steel, J. Electroanal. Chem., 832 (2019) 7-23.
6. S. Taguchi, M. Kondo, H. Mori, A. Aramata, Formation of zinc–oxianion complex adlayer by underpotential deposition of Zn on Au(111) electrode: Preferential formation of zinc monohydrogen phosphate complex in weakly acidic solutions, Electrochim. Acta, 111 (2013) 642-655.
7. J.O'M. Bockris, A.K.N. Reddy, M. Gamboa-Aldeco, Modern Electrochemistry, 2nd Ed., Vol. 2A, Kluwer Academic/ Plenum Publishers, 2000.
8. İ.Y. Erdoğan, T. Öznülüer, F. Bülbül, Ü. Demir, Characterization of size-quantized PbTe thin films synthesized by an electrochemical co-deposition method, Thin Solid Films, 517 (2009) 5419-5424.
9. I. Sisman, M. Alanyalioglu, U. Demir, Atom-by-Atom Growth of CdS Thin Films by an Electrochemical Co-deposition Method: Effects of pH on the Growth Mechanism and Structure, J. Phys. Chem. C, 111 (2007) 2670-2674.
10. T. Oznuluer, I. Erdogan, I. Sisman, U. Demir, Electrochemical atom-by-atom growth of PbS by modified ECALE method, Chem. Mater. 17 (2005) 935-937.
11. X. Zhang, X. Shi, C. Wang, Optimization of electrochemical aspects for epitaxial depositing nanoscale ZnSe thin films, J. Solid State Electrochem., 13 (2009) 469-475.
12. J.L. Stickney, The Chalkboard: Electrochemical Atomic Layer Deposition, Electrochem. Soc. Interf., 20 (2011) 28-30.
13. V. Sudha, M.V. Sangaranarayanan, Underpotential deposition of metals – Progress and prospects in modelling, J. Chem. Sci., 117 (2005) 207-218.
14. İ. Şişman, Ü. Demir, Electrochemical growth and characterization of size-quantized CdTe thin films grown by underpotential deposition, J. Electroanal. Chem, 651 (2011) 222-227.
15. J. Puiso, S. Tamulevicius, G. Laukaitis, S. Lindroos, M. Leskela, V. Snitka, Growth of PbS thin films on silicon substrate by SILAR technique, Thin Solid Films, 403 (2002) 457-461.
16. M. Biçer, A.O. Aydın, İ. Şişman, Electrochemical synthesis of CdS nanowires by underpotential deposition in anodic alumina membrane templates, Electrochim. Acta, 55 (2010) 3749-3755.
17. D. Fernando, M. Khan, Y. Vasquez, Control of the crystalline phase and morphology of CdS deposited on microstructured surfaces by chemical bath deposition, Mater. Sci. Semicond. Process., 30 (2015) 174-180.
18. W. Zhu, J.Y. Yang, X.H. Gao, J. Hou, S.Q. Bao, X.A. Fan, The underpotential deposition of bismuth and tellurium on cold rolled silver substrate by ECALE, Electrochim. Acta, 50 (2005) 5465-5472.
19. S. Cheng, G. Chen, Y. Chen, C. Huang, Effect of deposition potential and bath temperature on the electrodeposition of SnS film, Opt. Mater., 29 (2006) 439-444.
20. M.E. Hyde, R.G. Compton, A review of the analysis of multiple nucleation with diffusion controlled growth, J. Electroanal. Chem., 549 (2003) 1-12.
21. H.V.M. Hamelers, A. ter Heijne, N. Stein, R.A. Rozendal, C.J.N. Buisman, Butler–Volmer–Monod model for describing bio-anode polarization curves, Bioresour. Technol., 102 (2011) 381-387.
22. U. Demir, C. Shannon, Electrochemistry of Cd at (√3×√3) R30°-S/Au(111): Kinetics of Structural Changes in CdS Monolayers, Langmuir, 12 (1996) 6091-6097.
23. M.H. Hölzle, C.W. Apsel, T. Will, D.M. Kolb, Copper Deposition onto Au(111) in the Presence of Thiourea, J. Electrochem. Soc., 142 (1995) 3741-3749.
24. F.G. Cottrell, Der reststrom bei galvanischer polarisation, betrachtet als ein diffusionsproblem, Z. Physik Chem., 42 (1902) 385-431.
25. I. Petersson, E. Ahlberg, Kinetics of the electrodeposition of Pb□Sn alloys: Part I. At glassy carbon electrodes, J. Electroanal. Chem., 485 (2000) 166-177.